AMERICAN SOCIETY FOR MICROBIOLOGY | Journal of Virology®

VIRUS-CELL INTERACTIONS

Heterogeneous Nuclear Protein U Degraded the m^{6}A Methylated TRAF3 Transcript by YTHDF2 To Promote Porcine Epidemic Diarrhea Virus Replication

Hongchao Zhou,[a] Yuchao Yan,[a] Jie Gao,[a] Mingrui Ma,[a] Yi Liu,[a] Xiaojie Shi,[a] Qi Zhang,[a] Xingang Xu[a]

[a]College of Veterinary Medicine, Northwest A&F University, Yangling, Shaanxi, China

Hongchao Zhou and Yuchao Yan contributed equally to this work. Author order was determined in order of decreasing seniority.

ABSTRACT Porcine epidemic diarrhea virus (PEDV) belongs to the genus *Alphacoronavirus* of the Coronaviridae family and can cause fatal watery diarrhea in piglets, causing significant economic losses. Heterogeneous nuclear protein U (HNRNPU) is a novel RNA sensor involved in sensing viral RNA in the nucleus and mediating antiviral immunity. However, it remains elusive whether and how cytoplasmic PEDV can be sensed by the RNA sensor HNRNPU. In this study we determined that HNRNPU was the binding partner of Nsp13 by immunoprecipitation-liquid chromatography-tandem mass spectrometry (IP/LC-MS/MS) analysis. The interaction between Nsp13 and HNRNPU was demonstrated by using coimmunoprecipitation and confocal immunofluorescence. Next, we identified that HNRNPU expression is significantly increased during PEDV infection, whereas the transcription factor hepatocyte nuclear factor 1α (HNF1A) could negatively regulate HNRNPU expression. HNRNPU was retained in the cytoplasm by interaction with PEDV Nsp13. We found that HNRNPU overexpression effectively facilitated PEDV replication, while knockdown of HNRNPU impaired viral replication, suggesting a promoting function of HNRNPU to PEDV infection. Additionally, HNRNPU was found to promote PEDV replication by affecting TRAF3 degradation at the transcriptional level to inhibit PEDV-induced beta interferon (IFN-β) production. Mechanistically, HNRNPU downregulates TRAF3 mRNA levels via the METTL3-METTL14/YTHDF2 axis and regulates immune responses through YTHDF2-dependent mRNA decay. Together, our findings reveal that HNRNPU serves as a negative regulator of innate immunity by degrading TRAF3 mRNA in a YTHDF2-dependent manner and consequently facilitating PEDV propagation. Our findings provide new insights into the immune escape of PEDV.

IMPORTANCE PEDV, a highly infectious enteric coronavirus, has spread rapidly worldwide and caused severe economic losses. During virus infection, the host regulates innate immunity to inhibit virus infection. However, PEDV has evolved a variety of different strategies to suppress host IFN-mediated antiviral responses. Here, we identified that HNRNPU interacted with viral protein Nsp13. HNRNPU protein expression was upregulated, and the transcription factor HNF1A could negatively regulate HNRNPU expression during PEDV infection. HNRNPU also downregulated TRAF3 mRNA through the METTL3-METTL14/YTHDF2 axis to inhibit the production of IFN-β and downstream antiviral genes in PEDV-infected cells, thereby promoting viral replication. Our findings reveal a new mechanism with which PEDV suppresses the host antiviral response.

KEYWORDS PEDV, IFN-β, HNRNPU, TRAF3, YTHDF2, m^{6}A

Porcine epidemic diarrhea (PED) is a highly contagious intestinal infectious disease caused by the porcine epidemic diarrhea virus (PEDV), which is characterized by vomiting, watery diarrhea, anorexia, and high mortality of suckling pigs (1). PEDV is a

Editor Tom Gallagher, Loyola University Chicago

Address correspondence to Xingang Xu, tiger2003@nwsuaf.edu.cn, or Qi Zhang, zhangqi77@nwsuaf.edu.cn.

The authors declare no conflict of interest.

Received 12 November 2022
Accepted 6 January 2023
Published 8 February 2023

member of the genus *Alphacoronavirus* in the family Coronaviridae. Its genome is a single-stranded positive-strand RNA with a length of about 28 kb. The PEDV genome contains seven open reading frames (ORFs), encoding 16 nonstructural proteins (NSPs), an accessory protein (ORF3), and 4 structural proteins (SPs; containing an envelope, E; nucleocapsid, N; membrane, M; and spike, S). Nonstructural proteins are mainly hydrolyzed from the polyproteins pp1a and pp1b (2, 3). *In vitro*, a number of SPs and NSPs will suppress type I/III interferon (IFN) responses (4). IFN exerts a predominant function in the innate immunity of the host, which accounts for the first-line defense to resist pathogenic microorganisms (5). Among the nonstructural proteins, Nsp13 protein inhibits type I interferon production by selectively degrading TBK1 via p62-dependent autophagy (6). Thus, Nsp13 plays an important role in the process of virus proliferation. However, the mechanism of interaction between PEDV Nsp13 and host proteins is not yet fully understood.

In mammals, multiple members of the heterogeneous nuclear protein (HNRNP) family perform different functions, such as RNA splicing, RNA transport, genomic stability, innate immune response, and SUMOylation (7–9). Most members of the HNRNP family are located primarily in the nucleus and can be translocated to the mitochondria, endoplasmic reticulum, or Golgi apparatus in the cytoplasm (10). In addition, the HNRNP family proteins also play an active role in affecting viruses. Among them, HNRNPA1 protein can bind to the RNA of the influenza virus and prevent nucleic acid from exiting the nucleus to inhibit the influenza virus (11); HNRNPL interacts with foot-and-mouth disease virus (FMDV) internal ribosome entry sites (IRES) to suppress FMDV replication by downregulating viral RNA synthesis (12). HNRNPU, also known as nuclear matrix protein-nuclear scaffold attachment factor (SAFA), has recently been identified as a novel nuclear RNA sensor. Upon recognition of viral double-stranded RNA (dsRNA), HNRNPU oligomerizes in the nucleus and acts as a superenhancer, promoting the activation of antiviral responses by interacting with chromatin remodeling complexes (13). However, the mechanism by which HNRNPU regulates PEDV replication is unclear.

N^6-methyladenosine (m^6A) in mRNA is the most abundant internal modification of mRNA, so it is an important regulatory mechanism that controls gene expression in various physiological processes (14). The methylation modification of m^6A is reversible, including methyltransferases (writers), demethylases (erasers), and methylated reading proteins (readers). Among them, methyltransferases include METTL3/14, WTAP, and KIAA1429, which mainly catalyze the m^6A modification of adenylate on mRNA (15). The demethylases include FTO and ALKHB5, which are responsible for the demethylation of bases that have undergone m^6A modification (16). The main function of reading proteins (the YTHDF family) is to recognize bases modified by m^6A, thereby activating downstream regulatory pathways such as RNA degradation and microRNA (miRNA) processing (17, 18). In recent years, RNA m^6A modification has been found to play a role in the replication of many viruses and the immune response to viral infection. This modification can affect viral replication and can be hijacked to evade host cellular immunity (19). However, the mechanism of m^6A modification in PEDV evasion of innate immunity is not completely understood.

In this study, we aimed to better understand the mechanism of host-PEDV infection interaction through immunoprecipitation-liquid chromatography-tandem mass spectrometry (IP/LC-MS/MS) screening. We found that PEDV Nsp13 was able to interact with HNRNPU. During PEDV infection, HNRNPU can transfer from nucleus to cytoplasm, and the transcription factor HNF1A could affect the expression of HNRNPU. We demonstrated that overexpression of HNRNPU inhibits type I interferon production and promotes the replication of PEDV, whereas knockdown of HNRNPU promotes type I interferon production and inhibits the replication of PEDV. In addition, HNRNPU interacts with TRAF3 to degrade TRAF3 mRNA in a YTHDF2-dependent manner and inhibit IFN-I signaling to promote PEDV replication. In conclusion, our study suggests that PEDV infection can promote HNRNPU transfer from nucleus to cytoplasm to interact with Nsp13 and reveals the mechanism by which HNRNPU regulates innate immunity and PEDV replication.

A

Protein identified	Protein description	Peptides	Intensity	MW [kDa]	Score
SPTBN1	Spectrin beta, non-erythrocytic 1	5	86299000	272.95	35.144
RPS8	Ribosomal protein S8	5	807520000	22.866	67.378
HNRNPU	Heterogeneous nuclear ribonucleoprotein U	6	445270000	89.025	78.062
HIST2H2BE	Histone cluster 2 H2B family member e	2	1165500000	13.92	38.219
EEF1D	Eukaryotic translation elongation factor 1 delta	2	86299000	28.626	12.725
HKDC1	Hexokinase domain containing 1	3	144640000	91.035	18.677

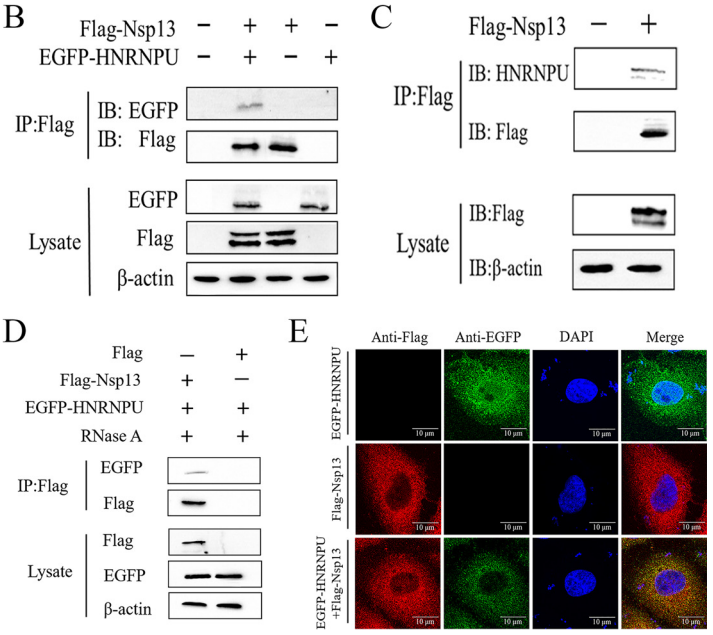

FIG 1 Interaction of HNRNPU with PEDV Nsp13 protein. (A) Summary of the PEDV Nsp13-interacting proteins identified by mass spectrometry. (B) Exogenous co-IP analysis of the binding of Nsp13 and HNRNPU. HEK293 cells were cotransfected with Flag-Nsp13 and EGFP-HNRNPU plasmids for 36 h. A quarter of the cell extract was subjected to the input assay to assess β-actin, Flag-fusion, and GFP-fusion protein levels. The rest of the extract was subjected to IP assay. Western blot analysis detected proteins with a mouse anti-GFP MAb and a mouse anti-Flag MAb. (C) An entire day of transfection of Marc-145 cells was accomplished using the Flag-Nsp13-encoding plasmids prior to the co-IP procedure, where the anti-Flag binding beads were utilized. Subsequently, Western blotting proceeded for investigating the protein precipitates. (D) The interaction of HNRNPU with PEDV Nsp13 protein after RNase treatment. (E) Following transfection of Marc-145 cells using HNRNPU-EGFP- and Nsp13-Flag-encoding plasmids, the specific primary and secondary antibodies were utilized to accomplish cellular labeling. DAPI labeling was used for the cellular nuclei. At the same time, confocal immunofluorescence microscopy was used to observe the fluorescent signals.

RESULTS

Identification of cellular proteins that interact with PEDV Nsp13 protein. To identify host cellular proteins that interact with PEDV Nsp13 protein, we employed immunoprecipitation-liquid chromatography-tandem mass spectrometry (IP/LC-MS/MS) analysis. Among these proteins, HNRNPU is a novel Nsp13-interacting protein. Because it scored highest among the identified candidate proteins, it was chosen for subsequent studies (Fig. 1A). Then, we sought to validate the interaction between HNRNPU and Nsp13 by immunoprecipitation (IP) assay *in vitro*. HEK293T cells were transfected with Flag-tagged-Nsp13 and enhanced green fluorescent protein (EGFP)-tagged-HNRNPU, individually or in combination. Cell lysates were immunoprecipitated with an anti-Flag monoclonal antibody (MAb), followed by Western blotting with mouse MAb against Flag or the EGFP tag. EGFP-tagged HNRNPU was coimmunoprecipitated with Flag-tagged Nsp13 when they were coexpressed but not in the absence of Nsp13, indicating that HNRNPU interacts with Nsp13 (Fig. 1B). Additionally, the PEDV Nsp13 protein contributed to the efficient coimmunoprecipitation with the endogenous HNRNPU protein (Fig. 1C), and the interaction was not affected by cell lysis with RNase (Fig. 1D), indicating that the PEDV Nsp13 protein interaction with HNRNPU

does not depend on RNA. Next, we investigated the colocalization of HNRNPU and the PEDV Nsp13 protein with confocal microscopy. Marc-145 cells were cotransfected with EGFP-HNRNPU and Flag-Nsp13, and protein localization was examined after 24 h. A confocal immunofluorescence assay showed that the HNRNPU and Nsp13 proteins colocalized in the cytoplasm (Fig. 1E), which further fostered interaction between Nsp13 and HNRNPU. Thus, it was shown that HNRNPU could interact with the Nsp13 protein of PEDV.

HNRNPU is involved in the infection of PEDV. We have already shown that PEDV Nsp13 interacts with HNRNPU. However, whether PEDV infection or Nsp13 transfection could affect the expression of HNRNPU remains unknown. To determine whether HNRNPU is involved in PEDV infection, the transcriptional and expression levels of HNRNPU were determined in a Marc-145 cell. We found that the protein and mRNA levels of HNRNPU were significantly increased under PEDV infection in a time- (Fig. 2A and B) and dose-dependent manner (Fig. 2C and D). The interaction between PEDV Nsp13 and host factor HNRNPU prompts us to guess whether the PEDV Nsp13 protein could affect HNRNPU expression. As expected, transfection of Flag-Nsp13 plasmid significantly increased mRNA and protein expression of HNRNPU (Fig. 2E and F). It has recently been reported that HNRNPU is an RNA sensor in the nucleus (13), whereas PEDV is a cytoplasmic RNA virus. Therefore, we hypothesized that translocation of HNRNPU might be the critical step for cytoplasmic RNA virus recognition. To determine the distribution of HNRNPU in Marc-145 cells under PEDV infection, HNRNPU proteins were separated from nucleus and cytoplasm to examine the subcellular distribution of HNRNPU. As with previous reports, HNRNPU was mainly localized in the nucleus in the resting state (Fig. 2G), whereas HNRNPU accumulated in the cytoplasm under PEDV infection and almost disappeared in the nucleus 24 h after exposure to PEDV (Fig. 2G). Additionally, overexpression of PEDV Nsp13 was able to promote the accumulation of HNRNPU in the cytoplasm in Marc-145 cells (Fig. 2H). These data suggest that nucleocytoplasmic translocation of HNRNPU may be essential for recognition of PEDV infection.

HNF1A negatively regulates the expression of HNRNPU. To detect the transcription factors of HNRNPU, we analyzed the promoter activation of HNRNPU in PEDV infection. Luciferase assays indicated that PEDV infection could enhance the activity of the HNRNPU promoter (Fig. 3A). To find the essential cis-regulatory elements of the HNRNPU promoter, the regions −0.36, −0.76, −1.16, −1.56, and −1.96 k (K represents 1000 bp upstream of the promoter region) were segmented to construct the pGL4.10-basic vector, and their ability to direct luciferase expression in HEK293T cells was tested. As shown in Fig. 3B, the promoter activity peaked between −1.16 and −1.56 k, indicating the presence of key active sites in this region. To confirm the boundaries of the minimal HNRNPU promoter, we further truncated the gradient in the region and finally determined that nucleotides from −1.36 to −1.46 k showed increased luciferase expression (Fig. 3B). Together, these results indicate that the boundaries of the minimal HNRNPU core promoter are at positions −1.36 to −1.46 k.

To analyze the transcriptional regulation of the HNRNPU gene, we used the bioinformatic tools JASPAR and Gene Regulation to find transcription factors that bind to the −1.36 to −1.46 k region. As a result, the HNF1A binding site in this region was identified (Fig. 3C). To demonstrate whether HNF1A regulates the expression of HNRNPU, we deleted the predicted binding site of HNF1A based on the reporter plasmid D2, and the results showed that the promoter activity was significantly upregulated (Fig. 3D). In addition, we constructed an HNF1A eukaryotic expression plasmid and cotransfected Marc-145 cells with reporter plasmids D2 and D2-delete HNF1A site. The results showed that overexpression of HNF1A significantly downregulated the activity of the HNRNPU promoter (Fig. 3D). We also observed an increase in the abundance of HNF1A mRNA during PEDV infection (Fig. 3E). To confirm that HNF1A is involved in the regulation of HNRNPU expression, we constructed a Flag-HNF1A expression plasmid, and Western blot analysis showed that the HNF1A gene was successfully constructed (Fig. 3F). We found that after overexpression of HNF1A, HNRNPU protein and mRNA levels were significantly downregulated during PEDV infection (Fig. 3G and H). Overall, these results indicate that HNF1A negatively regulates the activity of the HNRNPU promoter, thereby inhibiting its expression.

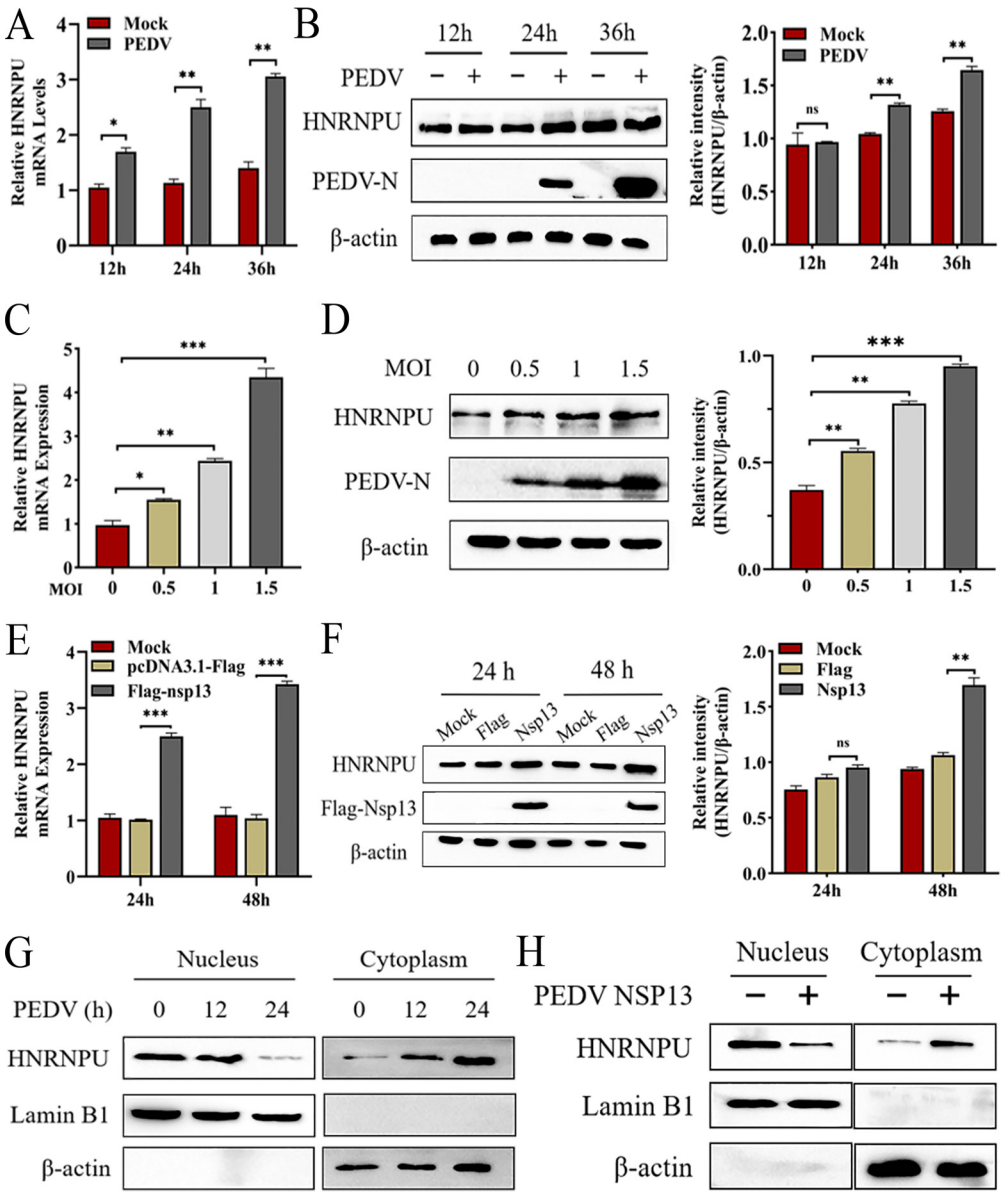

FIG 2 HNRNPU is involved in the infection of PEDV. (A) Marc-145 cells were infected with PEDV (MOI, 0.5) for 12, 24, or 36 h. HNRNPU mRNA was analyzed by qPCR. (B) Marc-145 cells were infected with PEDV (MOI, 0.5) for 12, 24, or 36 h. HNRNPU protein levels were analyzed by Western blotting. Western blot data were semiquantified and normalized against β-actin protein loading control. (C) Marc-145 cells were infected with PEDV (MOI, 0, 0.5, 1, 1.5) for 48 h. HNRNPU mRNA levels were analyzed by qPCR. (D) Marc-145 cells were infected with PEDV (MOI, 0, 0.5, 1, 1.5) for 24 h. HNRNPU protein levels were analyzed by Western blotting. Western blot data were semiquantified and normalized against β-actin protein loading control. (E) qPCR analysis of HNRNPU mRNA expression in Macr-145 cells transfected with Flag-Nsp13 plasmid at 24 h or 48 h posttransfection. (F) Immunoblot analysis of HNRNPU protein expression in Marc-145 cells transfected with Flag-Nsp13 plasmid at 24 h or 48 h posttransfection. (G) Marc-145 cells were infected with PEDV (MOI, 0.5) for the indicated time. Nuclear and cytoplasmic proteins were separated. HNRNPU, Lamin B1, and β-actin protein levels were analyzed by Western blotting. Lamin B1 and β-actin were nuclear and cytoplasmic index proteins, respectively. Nuclear and cytoplasmic Western blot data were semiquantified and normalized against lamin B1 and β-actin protein loading control, respectively. (H) Marc-145 cells were transfected with Flag-tagged PEDV Nsp13 for 24 h. The nuclear and cytoplasmic proteins were separated. HNRNPU, lamin B1, and β-actin protein levels were analyzed by Western blotting. Data were obtained from three independent experiments ($n = 3$). The differences were evaluated using Student's t test; significant differences are denoted as follows: *, $P < 0.05$; **, $P < 0.01$; ***, $P < 0.001$.

HNRNPU can promote PEDV replication. To investigate whether HNRNPU affects PEDV replication, HNRNPU protein was overexpressed in Marc-145 cells for 24 h, and then the cells were infected with PEDV at a multiplicity of infection (MOI) of 0.5. The cells and supernatants were collected at various time points and PEDV N expression

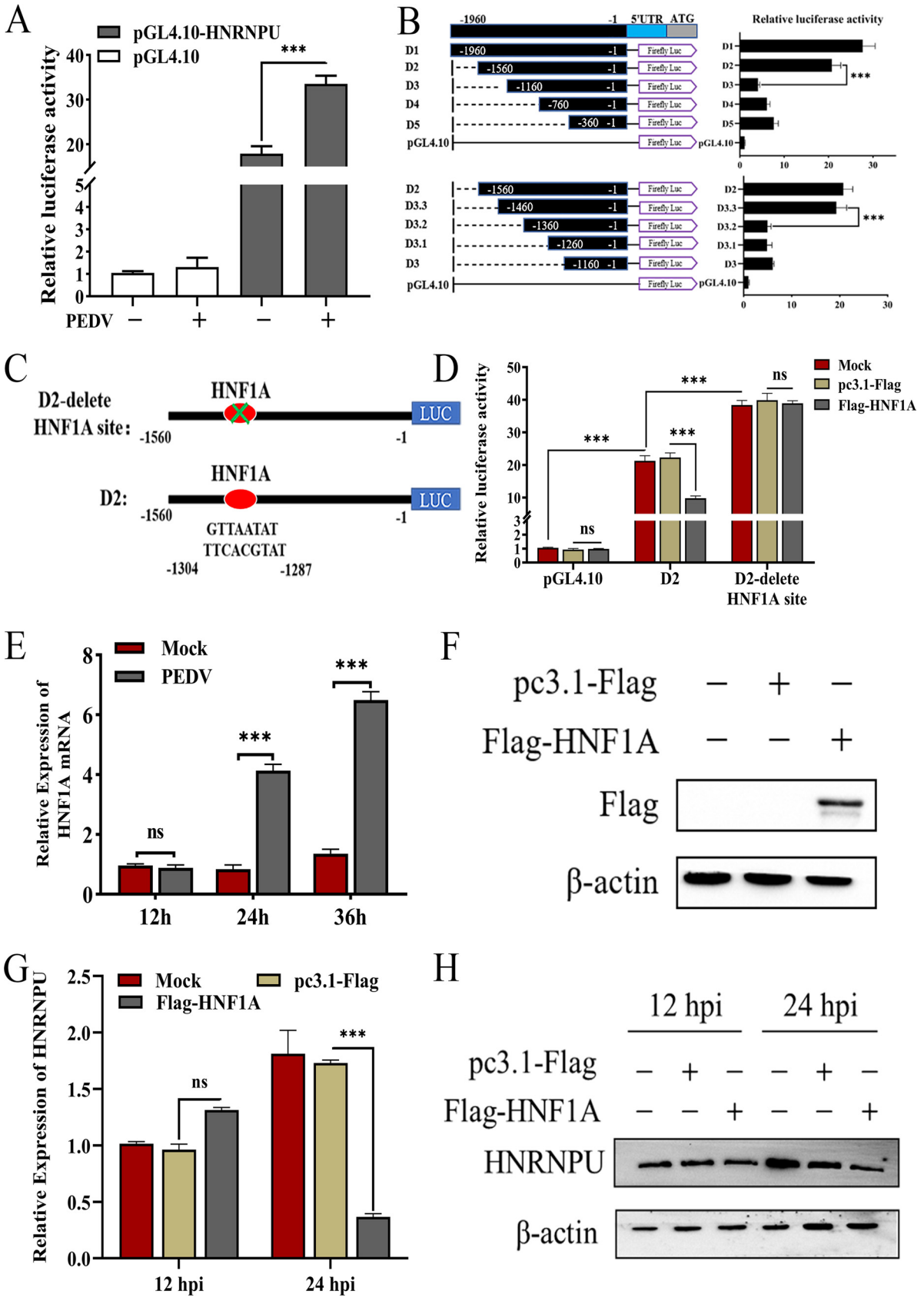

FIG 3 HNF1A is a new transcription factor of the HNRNPU gene. (A) Marc-145 cells were cotransfected with the promoter-reporter plasmids of HNRNPU and phRL-TK for 24 h, followed by infection with PEDV at an MOI of 1; the cells were harvested for dual-luciferase

(Continued on next page)

and PEDV viral loads were measured. Quantitative PCR (qPCR) and Western blot analysis indicated that overexpression of HNRNPU could significantly promote the replication of PEDV (Fig. 4A and B). In addition, the median tissue culture infective dose ($TCID_{50}$) was consistent with mRNA and protein results (Fig. 4C). To further verify the role of HNRNPU in PEDV replication, we designed small interfering RNA (siRNA) against HNRNPU and performed Western blotting to evaluate the interference efficiency of HNRNPU (Fig. 4D). As shown in Fig. 4E and F, PEDV N protein and mRNA levels in siHNRNPU cells were lower than those in normal control (NC)-siRNA transfected cells. Compared with the NC-si group, immunofluorescence assays exhibited fewer PEDV virions in siHNRNPU-transfected cells (Fig. 4G). Similarly, the virus titer in cells transfected with siHNRNPU was also reduced (Fig. 4H). In summary, these data indicate that HNRNPU positively regulates PEDV proliferation.

HNRNPU is not involved in PEDV attachment, internalization, or release. Having demonstrated that HNRNPU promotes PEDV infection, we next examined which stage of the viral life cycle was affected. Marc-145 cells were transiently transfected with EGFP-HNRNPU or siRNA targeting HNRNPU for 24 h and incubated with PEDV virions at an MOI of 10 for 1.5 h at 4°C to allow adsorption (see Fig. S1A in the supplemental material). For PEDV endocytosis, cells were subsequently switched from 4°C to 37°C for 1 h after removal of unbound virus. The cells were harvested for detection of PEDV N levels. The results showed that HNRNPU did not affect either adsorption or endocytosis of PEDV (Fig. S1B). As for the effect of HNRNPU on virus release, cells transfected with EGFP-HNRNPU and siHNRNPU were infected with PEDV at an MOI of 0.5 for 36 h, and virus release was calculated based on intracellular and extracellular virus N levels. HNRNPU does not affect PEDV release, as assessed by Western blot analysis (Fig. S1C). Based on the above-described results, we hypothesized that HNRNPU may participate in the PEDV genome replication stage by interacting with Nsp13.

HNRNPU negatively regulates type I IFN signaling. HNRNPU was reported to act as an RNA sensor in the nucleus or cytoplasm to activate IFN signaling following RNA virus infection (13). To examine the effect of HNRNPU on type I IFN signaling and antiviral immunity, we performed a dual luciferase reporter assay and found that ectopic expression of HNRNPU significantly suppressed the activation of IFN-β promoter and NF-κB promoter after intracellular (IC) poly(I·C) treatment (Fig. 5A). When we used siRNA to knock down HNRNPU, the activation of the IFN-β promoter and NF-κB promoter was significantly elevated (Fig. 5B). In addition, HNRNPU inhibited the activation of the IFN-β promoter and NF-κB promoter in a dose-dependent manner (Fig. 5C and D). Meanwhile, we performed qPCR analysis and found that overexpression of HNRNPU resulted in fewer IFN-β, interferon-stimulated gene 15 (ISG15), MX dynamin like GTPase 1 (Mx1), and interferon induced transmembrane protein 1 (IFITM1) mRNA during PEDV infection than in control cells (Fig. 5E). In contrast, the mRNA of IFN-β, ISG15, Mx1, and IFITM1 in siHNRNPU cells was higher than that in control cells (Fig. 5F). Together, these results suggest that HNRNPU negatively regulates type I interferon signaling and antiviral immunity.

HNRNPU targets TRAF3 and promotes its mRNA degradation. Host cells recognize incoming pathogen-associated molecular patterns (PAMPs) through multiple pattern recognition receptors (PRRs), such as Toll-like receptors (TLRs) and RIG-I-like receptors (RLRs). To clarify the molecular mechanism of HNRNPU-mediated antagonistic effects on the TLR or RLR signaling pathway, we first transfected plasmids encoding RIG-I, mitochondrial antiviral signaling protein (MAVS), TRAF3, or interferon regulatory factor (IRF3) together with the IFN-

FIG 3 Legend (Continued)
assays 24 h later. (B) Marc-145 cells were cotransfected with a different region of HNRNPU promoter-reporter plasmids and phRL-TK. The cells were harvested for dual-luciferase assays 48 h later. (C) The HNRNPU promoter region contains one HNF1A binding site. (D) Marc-145 cells were cotransfected with the indicated reporter plasmids and phRL-TK; the cells were harvested for dual-luciferase assays 48 h later. (E) Marc-145 cells were infected or mock infected with PEDV at an MOI of 0.5 and harvested at the indicated times. The expression of HNF1A was analyzed with real-time PCR. (F) Marc-145 cells were transfected with Flag empty plasmid and Flag-HNF1A plasmid for 48 h; the cells were harvested to detect the expression of HNF1A by Western blotting. (G and H) Marc-145 cells were transfected with Flag empty plasmid and Flag-HNF1A plasmid for 36 h, and infected with PEDV for 12 and 24 h. The cells were harvested to detect the expression of HNRNPU with Western blotting and qPCR. The differences were evaluated using Student's *t* test; significant differences are denoted as follows: *, $P < 0.05$; **, $P < 0.01$; ***, $P < 0.001$.

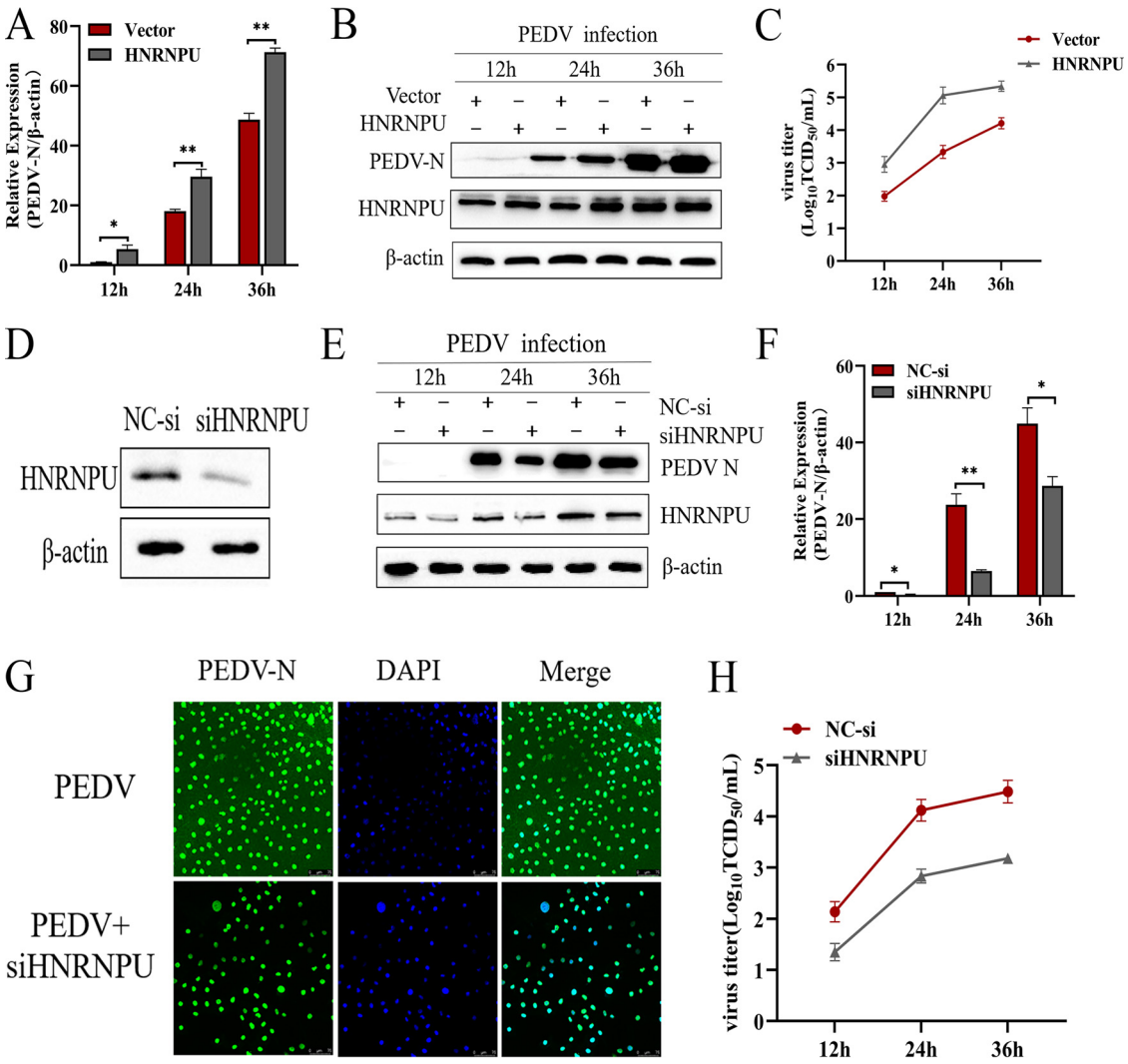

FIG 4 The HNRNPU protein affects PEDV replication. (A and B) Marc-145 cells were transfected with EGFP-HNRNPU or EGFP vector for 36 h. PEDV at an MOI of 1 was used to infect cells for 12, 24, or 36 h. Then, cells and supernatant were harvested to evaluate the mRNA and protein expression levels of PEDV-N by real-time PCR (A) and Western blotting (B). (C) The supernatant was harvested to assess viral title by $TCID_{50}$. (D) Marc-145 cells were transfected with siRNA for 48 h, and HNRNPU knockdown efficiency was assessed. (E and F) Marc-145 cells were transfected with siNC or siHNRNPU for 48 h, and cells were incubated with PEDV at an MOI of 1 for 12, 24, or 36 h. Then, qPCR and Western blotting detected PEDV-N mRNA (E) and protein expression (F). (G) Marc-145 cells were transfected with NC-si or si-HNRNPU and then infected with PEDV at an MOI of 0.5. Cells were fixed and incubated with mouse anti-PEDV polyclonal sera (1:500) at 24 h postinfection. Immunofluorescence assays were used to further observe intracellular propagation of PEDV. (H) PEDV titers in the culture supernatants were determined using the $TCID_{50}$ method. The differences were evaluated using Student's *t* test, and significant differences are denoted as follows: *, $P < 0.05$; **, $P < 0.01$; ***, $P < 0.001$.

β promoter in the presence or absence of HNRNPU. HNRNPU inhibited the activation of the IFN-β promoter triggered by the expression of RIG-I, MAVS, and TRAF3, but not IRF3 (Fig. 6A). Meanwhile, we found that overexpression of HNRNPU significantly reduced TRAF3 protein levels after PEDV infection (Fig. 6B) without affecting RIG-I and MAVS. Previously, we found that TRIM56 inhibited PEDV replication by enhancing the TLR3-TRAF3-mediated IFN-β antiviral response (20). Therefore, we overexpressed HNRNPU in Marc-145 cells and infected PEDV for 12 h, 24 h, and 36 h. It was found that HNRNPU did not affect the protein expression of TLR3 but could degrade the endogenous expression of TRAF3 (Fig. 6C). In order to verify whether TRAF3 interacts with HNRNPU during PEDV infection, Marc-145 cells were transfected with Flag-TRAF3- and EGFP-HNRNPU-expressing plasmids, and PEDV was infected for 24 h. The results showed that Flag-TRAF3 pulled down EGFP-HNRNPU (Fig. 6D). The confocal microscopic analysis further demonstrated that HNRNPU was colocalized with

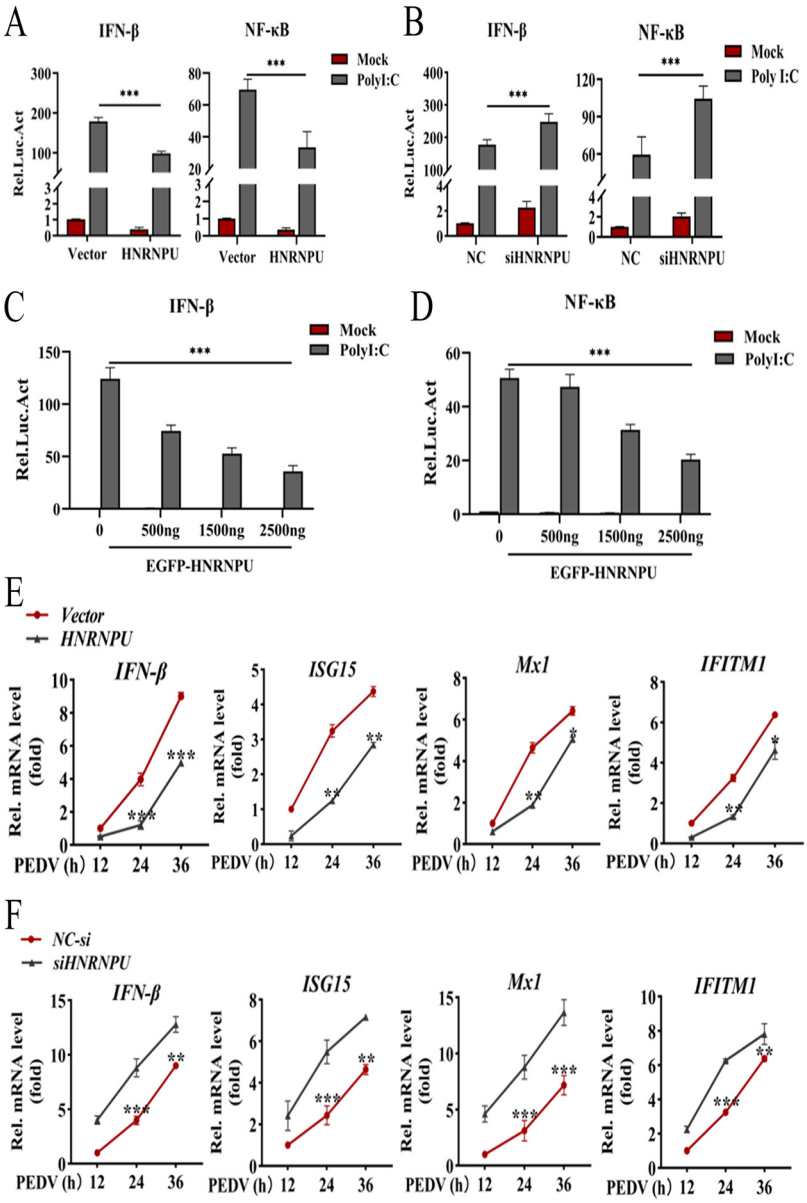

FIG 5 HNRNPU negatively regulates the type I IFN signaling pathway. (A and B) HNRNPU inhibits IFN-related promoter activities. Luciferase reporter plasmids (IFN-β-Luc or NF-κB-Luc) and the pRL-TK plasmid were cotransfected into HEK293 cells, along with EGFP-HNRNPU or Vec (A) or HNRNPU siRNA or scrambled siRNA (NC) (B). At 24 h after transfection, the cells were left untreated or were treated with poly(I·C) for 12 h before reporter assays were performed. (C and D) Luciferase reporter plasmids (IFN-β-Luc or NF-κB-Luc) and the pRL-TK plasmid were cotransfected into HEK293 cells, along with different concentrations of HNRNPU expression plasmid. At 24 h after transfection, cells were left untreated or were treated with poly(I·C) for 12 h before reporter assays. (E and F) Marc-145 cells were transfected with EGFP-HNRNPU or Vec (E) or HNRNPU siRNA or NC (F) and subsequently infected with PEDV for 12, 24, or 36 h before qPCR analysis. Data were obtained from three independent experiments ($n = 3$). The differences were evaluated using Student's t test; significant differences are denoted as follows: *, $P < 0.05$; **, $P < 0.01$; ***, $P < 0.001$.

TRAF3 mainly in the cytoplasm (Fig. 6E). These data indicate that HNRNPU protein can target TRAF3 for degradation and block interferon signal transduction.

It has been established that protein levels can be influenced by transcriptional or posttranslational modifications. To clarify whether HNRNPU affects TRAF3 degradation at the transcriptional or translational level, we detected the TRAF3 mRNA levels and found that overexpression of HNRNPU after PEDV infection significantly decreased TRAF3 mRNA (Fig. 6F). This indicated that the degradation of TRAF3 by HNRNPU

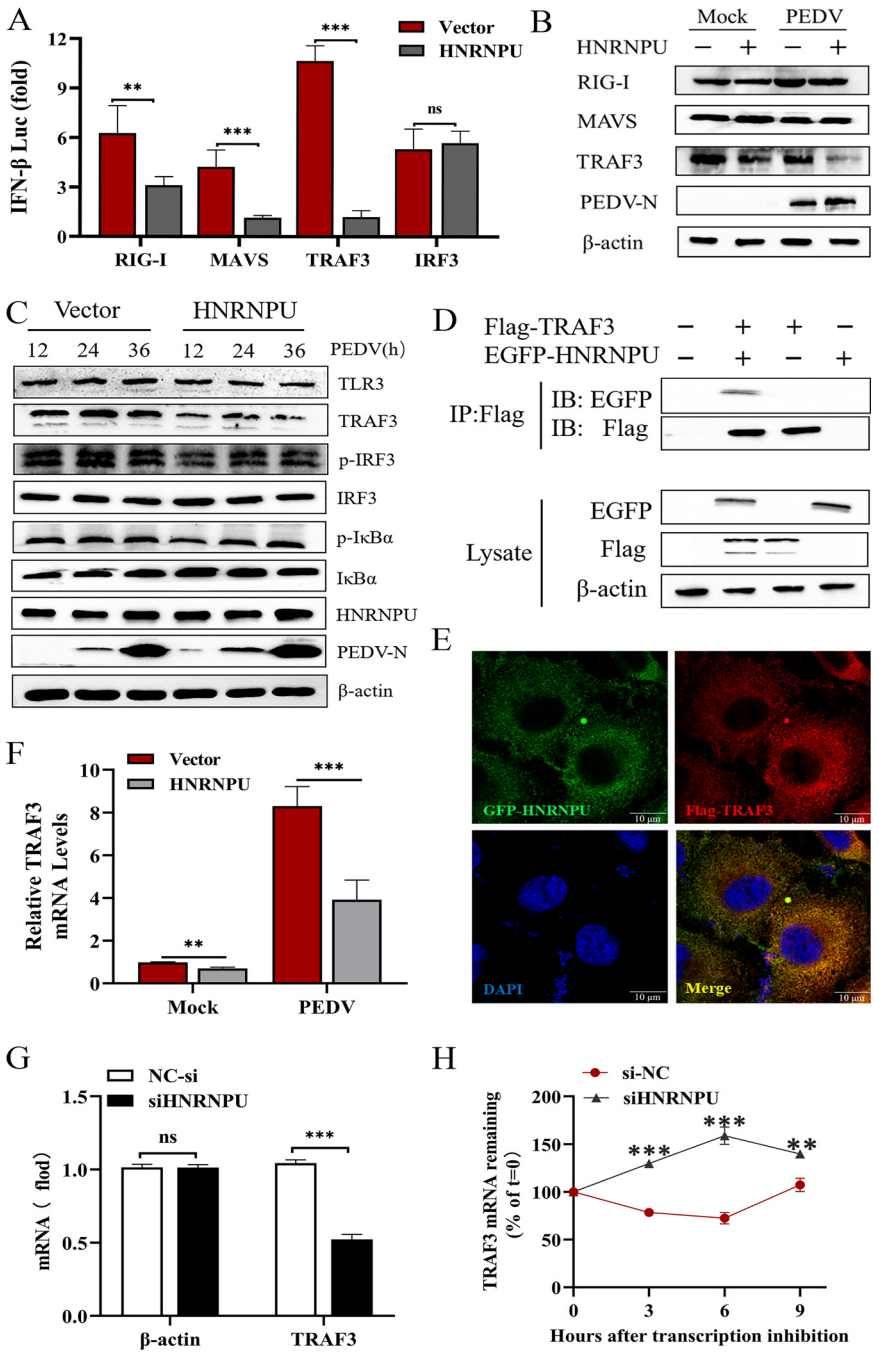

FIG 6 HNRNPU specifically interacts with TRAF3 and promotes mRNA degradation. (A) HNRNPU inhibits activation of the IFN-β promoter induced by RIG-I, MAVS, and TRAF3. HEK293T cells were transfected with the indicated plasmids along with control vector or HNRNPU expression plasmids. Reporter assays were performed 24 h after transfection. (B) Marc-145 cells were transfected with EGFP-HNRNPU and Flag-TRAF3 alone or cotransfected for 48 h. Cell samples were harvested, and the ectopically expressed TRAF3 was determined by Western blot analysis using antibodies against Flag tags. (C) Marc-145 cells were transfected with EGFP-HNRNPU for 36 h and then inoculated with PEDV for 12, 24, or 36 h. The expression of endogenous TRAF3 was determined by Western blot analysis. (D) Co-IP analysis of HNRNPU and TRAF3. Marc-145 cells were transfected with EGFP-HNRNPU and Flag-TRAF3 for 36 h, and PEDV was infected for 24 h. (E) The colocalization of HNRNPU and TRAF3 was observed by confocal immunofluorescence microscopy. (F) TRAF3 mRNA levels in PEDV infection after HNRNPU overexpression were detected by qPCR. (G) Detection of m^{6}A levels of TRAF3 in the siHNRNPU cells by MeRIP-qPCR. (H) TRAF3 mRNA degradation in PEDV-infected siHNRNPU Marc-145 cells treated with actinomycin D at the indicated times (n = 3), with the HNRNPU wild-type (WT) cells as the control. Residual RNAs were normalized to 0 h. Data were obtained from three independent experiments (n = 3). The differences were evaluated using Student's t test; significant differences are denoted as follows: *, $P < 0.05$; **, $P < 0.01$; ***, $P < 0.001$.

occurred at the transcriptional level. Previous studies have shown that cytoplasmic m^{6}A-methylated mRNA binds to cytoplasmic reader protein, affecting mRNA stability, translation, or localization (16). Using SRAMP and RMBasev2.0, we inferred that there were three m^{6}A modification sites (23 bp, 1,621 bp, and 1,639 bp) in the coding region of TRAF3 (Fig. S2A). MeRIP-qPCR further demonstrated that the m^{6}A level of TRAF3 was significantly decreased after siHNRNPU (Fig. 6G). In contrast, overexpression of HNRNPU significantly increased TRAF3 m^{6}A levels (Fig. S2B). The measurement of TRAF3 mRNA decay after blocking new RNA synthesis with actinomycin D showed that the stability of TRAF3 transcripts was significantly increased in silencing HNRNPU cells (Fig. 6H). Overexpressing HNRNPU significantly reduced TRAF3 mRNA stability (Fig. S2C). Taken together, these results confirm that HNRNPU inhibits innate immunity and promotes viral replication by affecting the stability of TRAF3 mRNA and reducing its protein expression during viral infection.

HNRNPU promotes RNA decay of TRAF3 in a YTHDF2-dependent manner. m^{6}A is mainly formed by METTL3-METTL14 heterodimers in mRNA transcripts, and the YTHDF2 protein is a crucial reader protein for RNA transcript m^{6}A methylation and promotes cytoplasmic mRNA degradation (21). We constructed METTL3, METTL14, and YTHDF2 protein expression plasmids. We found that overexpression of METTL3, METTL14, or YTHDF2 in Marc-145 cells significantly downregulated the mRNA levels of TRAF3, IFN-β, ISG15, and Mx1, which was consistent with the regulation mode of HNRNPU (Fig. 7A). We knocked down METTL3, METTL14, or YTHDF2 by siRNA-mediated silencing to confirm our hypothesis further. The results showed that silencing METTL3, METTL14, or YTHDF2 significantly upregulated the mRNA levels of TRAF3, IFN-β, ISG15, and Mx1 in Marc-145 cells (Fig. 7B).

To confirm the association between HNRNPU- and METTL3-METTL14/YTHDF2-mediated regulation of the transcripts, we found that silencing METTL3, METTL14, or YTHDF2 blocked the downregulation of the mRNA levels of TRAF3 and IFN-β by overexpressing HNRNPU in Marc-145 cells, but the N gene showed opposite changes, which implied that HNRNPU regulated the above-named transcripts via the METTL3-METTL14/YTHDF2 axis (Fig. 7C). We further found the same results at the protein level (Fig. 7D) and $TCID_{50}$ (Fig. 7E). We have shown that PEDV infection can cause HNRNPU nucleocytoplasmic translocation, and YTHDF2 is also a cytoplasmic protein. We speculated whether YTHDF2 also interacts with HNRNPU. The coimmunoprecipitation (co-IP) assay indicted that HNRNPU can bind to YTHDF2, and YTHDF2 facilitated efficient coimmunoprecipitation with HNRNPU (Fig. 7F and G). Moreover, the confocal immunofluorescence (IF) assay indicated that HNRNPU can colocalize with the YTHDF2 protein in the cytoplasm (Fig. 7H). Next, we aimed to determine the stability of the transcripts of TRAF3 using an RNA decay assay. We found that knockdown of YTHDF2 delayed the degradation of TRAF3 mRNA in overexpressing HNRNPU Marc-145 cells (Fig. 7I). In summary, these results indicate that HNRNPU promotes RNA decay of TRAF3 transcripts in a YTHDF2-dependent manner, thereby promoting PEDV replication.

Effect of the METTL3-METTL14/YTHDF2 axis on PEDV replication. The m^{6}A mechanism plays an important role in virus replication. However, the role of the METTL3-METTL14/YTHDF2 axis in porcine epidemic diarrhea virus replication remains unclear. First, we detected the mRNA and protein expression of the METTL3-METTL14/YTHDF2 axis in PEDV-infected Marc-145 cells. The results showed that mRNA and protein levels of METTL3, METTL14, and YTHDF2 increased when PEDV infected Marc-145 cells (Fig. 8A and B). To further elucidate the role of METTL3, METTL14, and YTHDF2 in PEDV replication, we transfected Marc-145 cells with siRNA of METTL3, METTL14, or YTHDF2 and then infected PEDV at 24 h. The interference efficiency is shown in Fig. 8C. qPCR results showed that at the mRNA level, siMETTL3 and siYTHDF2 significantly inhibited the PEDV N gene, while siMETTL14 had no significant effect on the PEDV N gene (Fig. 8D). Western blotting showed that the PEDV N protein was inhibited to various degrees after siMETTL3 and siYTHDF2. In contrast, the PEDV N protein level showed a slight increase after siMETTL14 (Fig. 8E). In conclusion, the YTHDF2 protein has a positive regulatory effect on PEDV replication, which is consistent with previous experimental results.

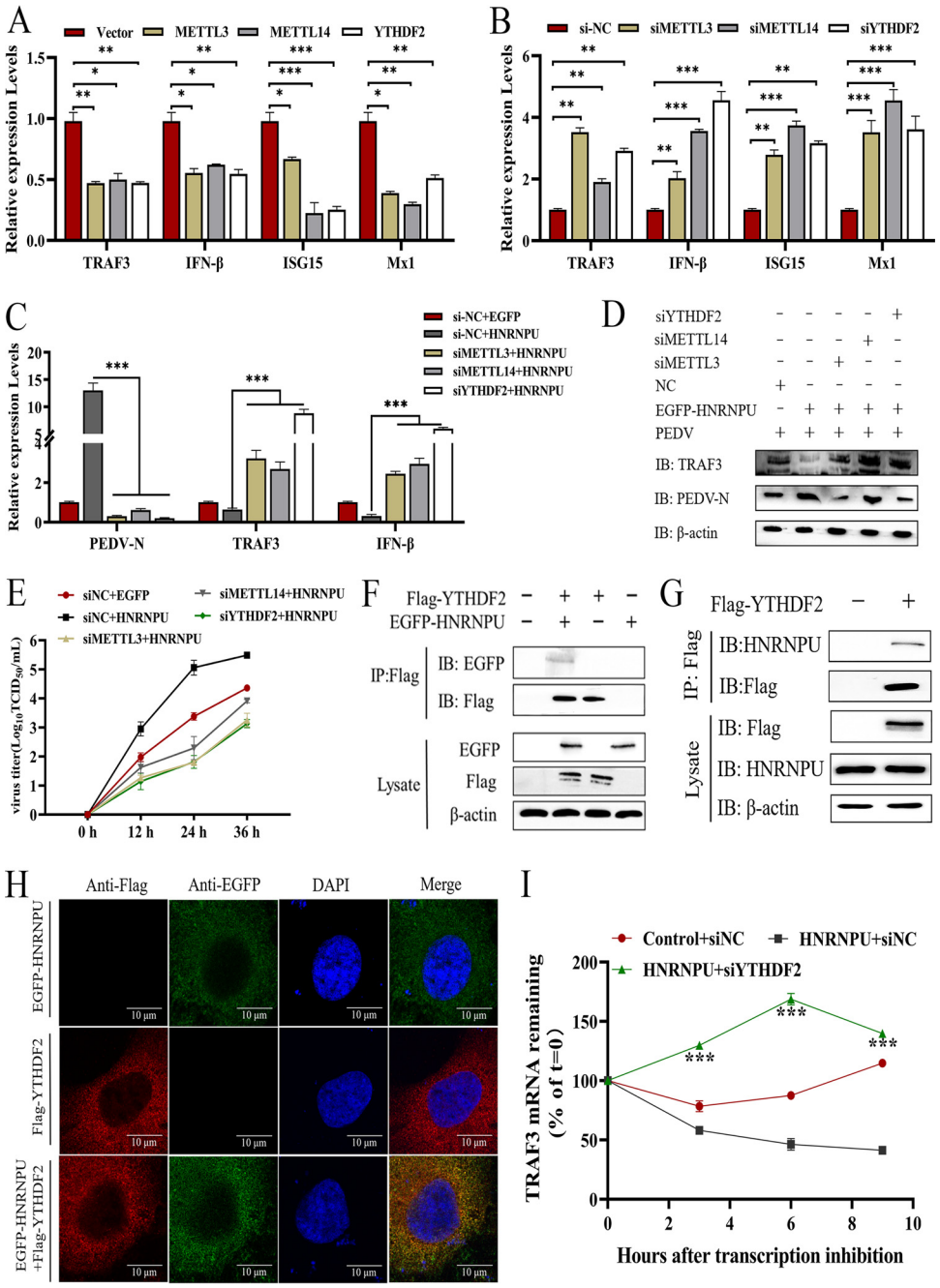

FIG 7 HNRNPU promotes RNA decay of TRAF3 in a YTHDF2-dependent manner. (A) Marc-145 cells were transfected with METTL3, METTL14, and YTHDF2 expression plasmid or empty vector. At 36 h after transfection, cells were stimulated with poly(I·C) for 24 h. (B) Marc-145 cells were transfected with siRNA targeting METTL3, METTL14, or YTHDF2 or with scrambled siRNA for 36 h. Cells were stimulated with poly(I·C) for 24 h and harvested. (C to E) Marc-145 cells were transfected with siRNA targeting YTHDF2, METTL3, or METTL14 or with scrambled siRNA for 24 h. Then, the cells were transfected with EGFP-HNRNPU expression plasmid or empty vector. At 48 h after transfection, cells were infected with PEDV and harvested at the indicated time. qPCR, immunoblotting, and $TCID_{50}$ were used for analysis. (F) Marc-145 cells were transfected with the indicated plasmids, and PEDV was inoculated for 24 h. Cell lysates were immunoprecipitated with Flag or EGFP antibodies, followed by immunoblotting with EGFP and Flag antibodies. (G) Marc-145 cells were transfected with Flag-YTHDF2 plasmid for a full day prior to PEDV infection, where the anti-Flag binding beads were utilized. Subsequently, Western blotting proceeded for investigating the protein precipitates. (H) Marc-145 cells were cotransfected with HNRNPU and YTHDF2 plasmids, and PEDV was infected for 24 h. The cells were then stained with anti-HNRNPU (green), anti-YTHDF2 (red), and DAPI (blue) immunofluorescence and analyzed under microscopes. (I) TRAF3 mRNA degradation in the indicated YTHDF2-silenced cells treated with actinomycin-D (n = 3). Residual RNAs were normalized to 0 h. Cells were transfected with YTHDF2 siRNA (siNC) for 24 h, transfected with HNRNPU (control vector) for 24 h, infected with PEDV, and then treated with actinomycin D at

(Continued on next page)

DISCUSSION

Virus helicase plays an important role in virus infection, viral genome replication, and transcription (22, 23). During replication of an RNA virus, the helicase must efficiently unwind the viral dsRNA replication intermediates to release the newly synthesized progeny viral RNA from the template RNA (24, 25). Therefore, the ATPase and helicase activities of PEDV Nsp13 are necessary for progeny virus synthesis. However, there are relatively few studies on the PEDV Nsp13 protein. It is very important to analyze the host protein interacting with it to understand the pathogenesis of the virus. In this study, we identified the host cell protein HNRNPU as an interacting partner of Nsp13 protein by IP/LC-MS/MS analysis. The interaction between Nsp13 and HNRNPU was demonstrated by using coimmunoprecipitation and confocal immunofluorescence.

As a novel nuclear RNA sensor, HNRNPU oligomerizes and interacts with SMARCA5 and TOP1, two key components of the nucleosome remodeling complex, to promote the activation of antiviral gene enhancers and superenhancers when viral RNA is detected in the nucleus (13). In addition, HNRNPU plays an antiviral role in limiting the replication of several viruses, including HSV-1 (26) and IBDV (27). However, the role of HNRNPU in PEDV remains largely unknown. This study was the first to show that PEDV infection and Nsp13 transfection upregulated the intracellular expression of HNRNPU in a time-and dose-dependent manner. Previous studies have shown that HNRNPU is a nuclear protein that does not shuttle between the nucleus and cytoplasm (28, 29). Here, we observed that PEDV promotes HNRNPU translocation, and PEDV Nsp13 is important for mediating HNRNPU translocation. These results suggest that nucleoplasmic translocation of HNRNPU may be critical for recognizing PEDV infection. The control of HNRNPU expression at the transcriptional level could indicate a deeply critical element for the pathogenesis of PEDV. To further identify the transcription factors that regulate HNRNPU expression, the HNRNPU promoter sequence was amplified. We found that the smallest HNRNPU core promoter is located between positions −1360 and −1460. Through the analysis of HNRNPU regulatory elements, we found that HNF1A can bind to the promoter of HNRNPU and then regulate HNRNPU expression.

The innate immune system is the host's first line of defense against virus invasion, and the antiviral response is mainly controlled by IFN, leading to the production of hundreds of interferon-stimulated genes (ISGs), thus forming the antiviral state (30). As a cytoplasmic RNA virus, PEDV is recognized by a variety of cytoplasmic RNA PRRs, such as TLR3 (31) or RIG-I and MDA5 (32). However, PEDV develops unique mechanisms to avoid the IFN effect by preventing the sensor from recognizing and binding to viral products and by degrading key proteins in the IFN signaling pathway. Studies have shown that PEDV N protein circumvents host antiviral immunity by preventing TBK1 from interacting with IRF3, which is necessary for the activation of IFN production signaling (33). PEDV Nsp7 can inhibit interferon-induced JAK-STAT signaling by sequestering the interaction between KPNA1 and STAT1 (34). Furthermore, viral helicases may modulate the innate immune response of the host. For example, the interaction between porcine reproductive and respiratory syndrome virus (PRRSV) helicase (Nsp10) and host DEAD box RNA helicase 18 can promote PRRSV replication (35). West Nile virus (WNV) helicase Nsp3 plays a role in inhibiting type I interferon signaling (36). The interaction of the infectious bronchitis virus (IBV) helicase Nsp13 with the p125 subunit of DNA polymerase δ facilitates viral replication (37). However, little is known about the role of PEDV helicase Nsp13 in regulating type I interferon production. In this study, we found that the upregulation of HNRNPU, an RNA sensor in the cytoplasm, after PEDV infection and Nsp13 transfection could reduce the protein expression of TRAF3, thereby reducing the phosphorylation of IRF3 and the expression of downstream interferon-stimulated genes.

FIG 7 Legend (Continued)
the indicated times ($n = 3$). Residual RNAs were normalized to 0 h. Data were obtained from three independent experiments ($n = 3$). The differences were evaluated using Student's t test; significant differences are denoted as follows: *, $P < 0.05$; **, $P < 0.01$; ***, $P < 0.001$.

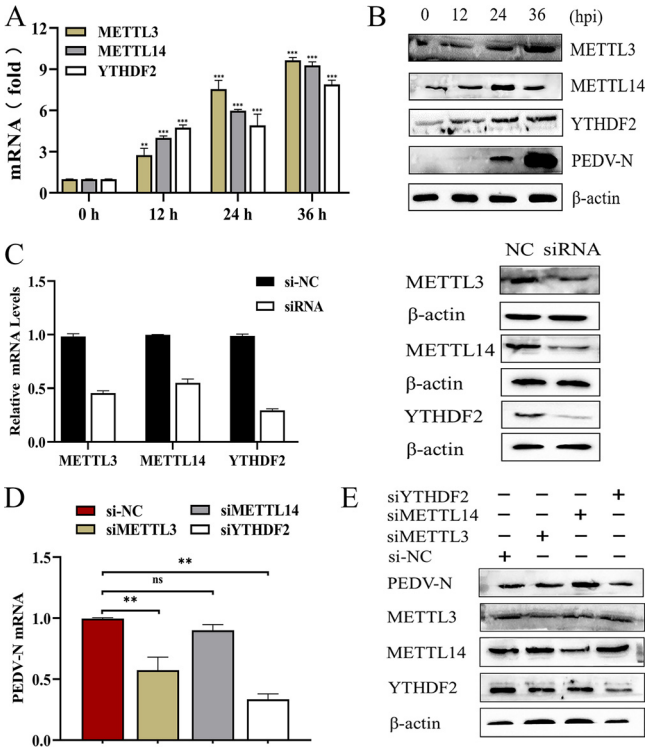

FIG 8 Effect of the METTL3-METTL14/YTHDF2 axis on PEDV replication. (A and B) Marc-145 cells were infected with PEDV at an MOI of 0.5. At 0 h, 12 h, 24 h, and 36 h after infection, the mRNA and protein expression levels were detected. (C) Marc-145 cells were transfected with siRNA for 48 h, and knockdown efficiency was assessed. (D and E) Marc-145 cells were transfected with siRNA for 36 h. PEDV at an MOI of 1 was used to infect cells for 24 h. Then, cells and supernatant were harvested to evaluate the mRNA and protein expression level of PEDV-N by real-time PCR (D) and Western blotting (E). Data were obtained from three independent experiments ($n = 3$). The differences were evaluated using Student's *t* test; significant differences are denoted as follows: *, $P < 0.05$; **; $P < 0.01$; ***, $P < 0.001$.

Mammalian mRNAs can be modified by a variety of chemical modifications such as N^6-methyladenosine (m^6A), 5-methlcytidine, and inosine, in addition to N^7-methylguanosine, which is part of the 5′-terminal cap (38). Among various internal chemical modifications of RNA, m^6A RNA methylation is the most common mRNA modification. A methyltransferase complex consisting of METTL3, METTL14, and WTAP cotranscribes m^6A on mRNA. This modification is usually enriched near the 3′ untranslated region (UTR) and stop codons of cellular mRNAs (39). The m^6A-modified mRNA is especially recognized by YTH domain family proteins (YTHDF1, YTHDF2, and YTHDF3) to regulate mRNA stability, translation, and localization (17, 40). At present, there are relatively few studies on the regulation and mechanism of m^6A modification on viral replication. It has been found that YTHDF protein can inhibit hepatitis C virus (HCV) virion production by competing with viral RNA for nucleocapsid protein (41). DDX5 promotes viral infection by inhibiting antiviral innate immunity by interacting with METTL3 and modulating m^6A levels on DHX58 and NF-κB transcripts (42). DDX46 inhibits innate immunity in the nucleus by trapping m^6A, a demethylated antiviral transcript (19). However, the relationship between PEDV and m^6A modification remains unclear. Currently, it is known that m6A demethylase ALKBH5 inhibits PEDV infection by regulating GAS6 expression in porcine alveolar macrophages (43). In the study, we found that HNRNPU caused the degradation of TRAF3 mRNA through the METTL3-METTL14/YTHDF2 axis, thereby reducing its protein expression to inhibit innate immunity and promote PEDV replication.

In summary, we first identified the new interacting protein HNRNPU of PEDV Nsp13 through IP/LC-MS/MS analysis. Furthermore, we found that PEDV infection upregulated the expression level of HNRNPU protein and was regulated by its transcription factor

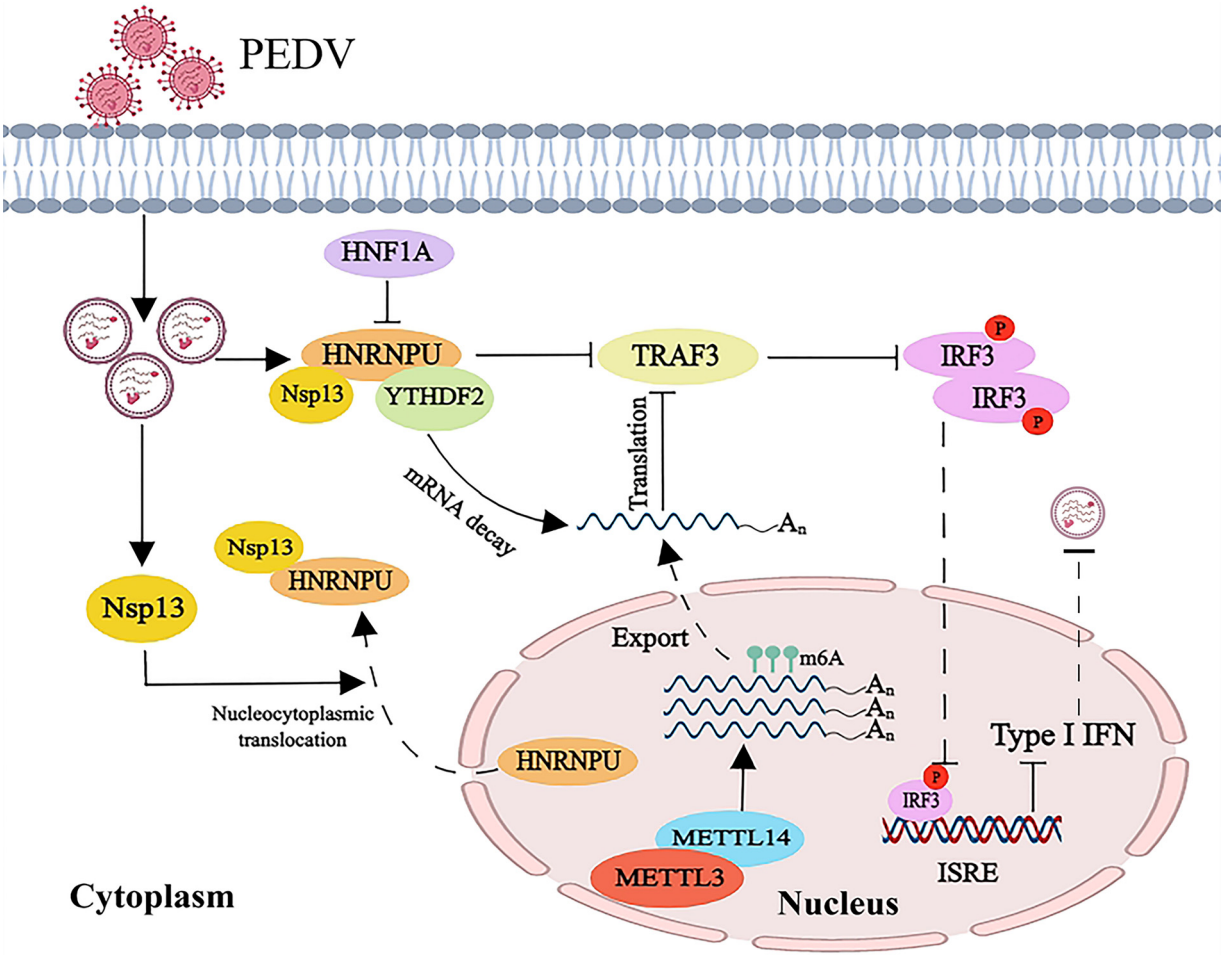

FIG 9 Working model for the mechanism through which HNRNPU inhibits antiviral innate immunity by promoting TRAF3 mRNA degradation. Under PEDV infection, HNRNPU is retained in the cytoplasm through interaction with PEDV Nsp13. After modification by the m^{6}A "writer" complex METTL3/METTL14, TRAF3 is recognized by the m^{6}A reader protein and degraded in a YTHDF2-dependent manner, ultimately leading to inhibition of the antiviral pathway.

HNF1A. Mechanistically, our studies showed that HNRNPU can degrade TRAF3 transcripts in a YTHDF2-dependent manner, inhibit innate immunity, and promote PEDV replication (Fig. 9). Our study illustrates a new mechanism of HNRNPU regulation of PEDV, which helps us understand how PEDV evaded innate immunity through m^{6}A modification and provides a new and effective strategy for the control of PEDV infection in the future.

MATERIALS AND METHODS

Cell culture and transfection. We cultivated African green monkey kidney epithelial cells (Marc-145) and human embryonic kidney cells (HEK293T) cells in Dulbecco minimal essential medium (DMEM) (HyClone, Logan, UT, USA) supplemented with 10% fetal bovine serum (FBS; Gibco, Grand Island, NY, USA). The above-described cell lines were inoculated under 5% CO_2 and 37°C conditions. According to manufacturer's instructions, we used Lipo8000 transfection reagent (Beyotime Biotechnology, China) and transfected the plasmid into 6-well plates when the cell density reached 80% to 90%. In addition, siRNA was transfected into cells after they reached 50% to 60% confluence.

Viral infection and titration. The PEDV strain CH/SXYL/2016 (GenBank identifier [ID] MF462814.1) was isolated and stored in our laboratory (44). In the PEDV infection process, Marc-145 cells were washed three times with phosphate-buffered saline (PBS) and then infected at a multiplicity of infection (MOI) of 0.5 at 37°C. After 1 h, the unbound virus was removed, and the cells were cultured in 2% FBS at different time intervals until harvest. Cell culture supernatant was harvested at different hours postinfection (hpi), and virus titers were determined by Karber's method on Marc-145 cells.

Reagents and antibodies. The mouse polyclonal anti-PEDV N antibody was stocked in our laboratory (45). Antibodies against β-actin (AC026), IκBα (A19714), p-IκBα (AP0707), TLR3 (A11778), and TRAF3 (7187) were purchased from ABclonal Biotechnology. Anti-METTL3 (15073-1-AP), METTL14 (26158-1-AP),

TABLE 1 The sequences of the primers and siRNAs

Purpose	Name	Sequence (5′–3′)
Real-time PCR primers	PEDV N forward	AGATCGCCAGTTTAGCACCA
	PEDV N reverse	GGCAAACCCACATCATCGT
	mHNRNPU forward	ATACCCTCGTGCTCCTGT
	mHNRNPU reverse	CGATTGTTTCCTCGTCCT
	HNF1A forward	GGATGATACGGACGACGATG
	HNF1A reverse	GGTCTCCACCACGGCTTT
	ACTB forward	CTTAGTTGCGTTACACCCTTTC
	ACTB reverse	TGTCACCTTCACCGTTCCA
	TRAF3 forward	TTTGTGGCCCAGACTGTTCT
	TRAF3 reverse	TCCGAAGTATCCACTATGAC
	IFN-β forward	GCAATTGAATGGAAGGCTTGA
	IFN-β reverse	CAGCGTCCTCCTTCTGGAACT
siRNA sequences	si-HNRNPU	CGUGGUAGUUACUCAAACATT
	si-METTL3	GCAGTTCCTGAATTAGCTA
	si-METTL14	CCTCCTCCCAAATCTAAAT
	si-YTHDF2	GCCCAATAATGCGTATACT

YTHDF2 (24744-1-AP), MAVS (14341-1-AP), and RIG-I (20566-1-AP) were purchased from Proteintech. Anti-IRF3 (ET1612-14), anti-p-IRF3 (ET1608-22), and Flag (0912-1) antibodies were bought from Huaan Biological Technology (Hangzhou, China). HNRNPU (CY8112), GEP-tag (AB0005), and lamin B1 (AB0054) were purchased from Abways Technology. Anti-Flag-tag antibody was bought from TransGen Biotech (HT201-01). HRP-labeled anti-mouse (DY60203) and anti-rabbit (DY60202) IgG antibodies were acquired from Shanghai Diyi Biotechnology. The siRNA sequence was designed and synthesized by General Biol (Anhui, China). In addition, actinomycin D (HY-17559) was bought from MedChemExpress.

qPCR. Total cellular RNA was isolated from cells using TRNzol universal reagent (Tiangen, China). According to the manufacturer's instructions, 2 μg of total RNA was reverse-transcribed to cDNA using the FastKing reverse transcription (RT) kit with gDNase (Tiangen). Later, qPCR was conducted with the use of SYBR green select master mix (ABclonal). The 2-$\Delta\Delta^{CT}$ method was used to assess the mRNA levels. The gene-specific primers for qPCR are listed in Table 1.

Western blot analysis. Cells were harvested under different conditions. RIPA lysis and extraction buffer (PL006, Zhonghui Hecai, Shaanxi), including protease inhibitor (PL026) as well as phosphatase inhibitor (PL012-1) were used to lyse cell samples that were washed twice with PBS. Total protein concentration was measured using BCA protein assay (Pierce, Rockford, IL, USA). Equal amounts of protein were resolved by sodium dodecyl sulfate-polyacrylamide gel electrophoresis (SDS-PAGE). The proteins were then transferred onto polyvinylidene fluoride (PVDF) membranes (Millipore Corp, Atlanta, GA, USA). The membranes were treated with 5% fat-free milk powder (1172GR500, BioFroxx) for 1 hour and incubated with primary antibodies overnight at 4°C with a gentle shaking. Subsequently, the membrane was washed with 0.1% PBS with Tween 20 (PBST) for 15 min and incubated with the HRP-conjugated secondary antibodies at room temperature for 60 min. Finally, enhanced chemiluminescence (ECL; GE Healthcare) was used to measure the proteins.

Coimmunoprecipitation (co-IP) assays. The cells were cultured in a 10-cm cell plate and transfected with the indicated plasmids using Lipo8000 transfection reagent for 36 h. The cell lysate was added to the sample and lysed at 4°C for 30 min. Subsequently, it was centrifuged at 12,000 $\times$ *g* for 30 min at 4°C to obtain the lysate supernatant. The lysate supernatant was incubated with protein A/G-agarose (Santa Cruz, California, USA) at 4°C for 1.5 h. After centrifugation at 12,000 $\times$ *g* for 10 min, the supernatant was incubated with the primary antibody overnight at 4°C. Then, the protein A/G-agarose was added to the above-described mixture and incubated at 4°C for 6 h and then centrifuged at 12,000 $\times$ *g* for 1 min to obtain a precipitate. Finally, the protein was eluted by boiling it in a 5$\times$ loading buffer for 10 min and analyzed by Western blotting.

Dual-luciferase reporter assays. In this study, cells were seeded in 12-well plates, followed by transfection using the indicated plasmids, luciferase reporters, and pRL-TK by Lipo8000 (Beyotime Biotechnology, Shanghai, China). At 24 h posttransfection, cells were lysed and then analyzed using a dual-luciferase reporter assay kit (Promega, Beijing, China). Firefly luciferase and *Renilla* fluorescein protease activity were measured according to the instructions. The luciferase value was normalized with *Renilla* luciferase activity as an internal control. In addition, three independent experiments were carried out.

Methylated RNA immunoprecipitation coupled with qPCR (MeRIP-qPCR). After the cells were collected, they were washed 3 times with precooled PBS. Total RNA from the cells was extracted with TRIzol reagent according to manufacturer's instructions. The integrity of the RNA was detected with formaldehyde denatured agarose gel electrophoresis. The RNA was broken using a noncontact fully automatic ultrasonic crusher (Covaris, Woburn, MA, USA). A small portion (10%) of the RNA fragment was collected as an input sample (input). The fragment RNA was incubated and immunoprecipitated with m^{6}A antibody (Cell Signaling Technology, Danvers, MA, USA) at 4°C for 4 h. The m^{6}A antibody RNA mixture was incubated with protein A/G magnetic beads at 4°C for 2 h. RNA was extracted using TRIzol reagent, and m^{6}A enrichment was detected by qPCR.

Fluorescence microscopy. Cells were subjected to cotransfection with the indicated plasmids for 36 h. PBS was used to wash the cells, which were fixed in 4% paraformaldehyde (PFA; SL1830, Coolaber) for 15 min. They were then permeabilized using 0.1% Triton X-100 (T8200, Solarbio, Beijing, China) for 10 min at the ambient temperature. After being rinsed with PBS, the cells were incubated with the primary antibody for an hour at 37°C. The cells were rinsed with PBS and nurtured with fluorescent-labeled secondary antibodies for an hour at 37°C. In the end, we stained the cells with DAPI (4′,6-diamidino-2-phenylindole; BL105A, Biosharp) for 5 min at ambient temperature. The cells were then examined with a Leica TCS Sp8 microscope and a Nikon ECLIPSE Ti microscope.

Statistical analysis. All findings were for three independent experiments, and the data are presented as means ± standard deviations (SD). This study employed the Prism 7 software (GraphPad Software, USA) to carry out Student's *t* test (two-sided) as well as to detect significant differences between groups. The importance of the different groups was identified using a two-tailed Student's *t* test with the GraphPad Prism 7 software. *, $P < 0.05$; **, $P < 0.01$; ***, $P < 0.001$.

SUPPLEMENTAL MATERIAL

Supplemental material is available online only.

SUPPLEMENTAL FILE 1, PDF file, 0.5 MB.

ACKNOWLEDGMENTS

This work was supported by grants from the agricultural special fund project of Shaanxi Province (no. 2019SJNYZX45) and the innovation project for agrotechnology of Shaanxi Province (no. 2019NY-081), China.

We declare that we have no conflicts of interest.

REFERENCES

1. Jung K, Saif LJ. 2015. Porcine epidemic diarrhea virus infection: etiology, epidemiology, pathogenesis and immunoprophylaxis. Vet J 204:134–143. https://doi.org/10.1016/j.tvjl.2015.02.017.
2. Kocherhans R, Bridgen A, Ackermann M, Tobler K. 2001. Completion of the porcine epidemic diarrhoea coronavirus (PEDV) genome sequence. Virus Genes 23:137–144. https://doi.org/10.1023/a:1011831902219.
3. Duarte M, Gelfi J, Lambert P, Rasschaert D, Laude H. 1993. Genome organization of porcine epidemic diarrhoea virus. Adv Exp Med Biol 342:55–60. https://doi.org/10.1007/978-1-4615-2996-5_9.
4. Zhang Q, Yoo D. 2016. Immune evasion of porcine enteric coronaviruses and viral modulation of antiviral innate signaling. Virus Res 226:128–141. https://doi.org/10.1016/j.virusres.2016.05.015.
5. Tanji T, Ip YT. 2005. Regulators of the Toll and Imd pathways in the Drosophila innate immune response. Trends Immunol 26:193–198. https://doi.org/10.1016/j.it.2005.02.006.
6. Sui C, Xiao T, Zhang S, Zeng H, Zheng Y, Liu B, Xu G, Gao C, Zhang Z. 2022. SARS-CoV-2 NSP13 inhibits type I IFN production by degradation of TBK1 via p62-dependent selective autophagy. J Immunol 208:753–761. https://doi.org/10.4049/jimmunol.2100684.
7. Liu BY, Yu XJ, Zhou CM. 2021. SAFA initiates innate immunity against cytoplasmic RNA virus SFTSV infection. PLoS Pathog 17:e1010070. https://doi.org/10.1371/journal.ppat.1010070.
8. Zietzer A, Hosen MR, Wang H, Goody PR, Sylvester M, Latz E, Nickenig G, Werner N, Jansen F. 2020. The RNA-binding protein hnRNPU regulates the sorting of microRNA-30c-5p into large extracellular vesicles. J Extracell Vesicles 9:1786967. https://doi.org/10.1080/20013078.2020.1786967.
9. Santos-Pereira JM, Herrero AB, Garcia-Rubio ML, Marin A, Moreno S, Aguilera A. 2013. The Npl3 hnRNP prevents R-loop-mediated transcription-replication conflicts and genome instability. Genes Dev 27:2445–2458. https://doi.org/10.1101/gad.229880.113.
10. Xie W, Zhu H, Zhao M, Wang L, Li S, Zhao C, Zhou Y, Zhu B, Jiang X, Liu W, Ren C. 2021. Crucial roles of different RNA-binding hnRNP proteins in stem cells. Int J Biol Sci 17:807–817. https://doi.org/10.7150/ijbs.55120.
11. Kaur R, Batra J, Stuchlik O, Reed MS, Pohl J, Sambhara S, Lal SK. 2022. Heterogeneous ribonucleoprotein A1 (hnRNPA1) interacts with the nucleoprotein of the influenza A virus and impedes virus replication. Viruses 14:199. https://doi.org/10.3390/v14020199.
12. Sun C, Liu MM, Chang JT, Yang DC, Zhao B, Wang HW, Zhou GH, Weng CJ, Yu L. 2020. Heterogeneous nuclear ribonucleoprotein L negatively regulates foot-and-mouth disease virus replication through inhibition of viral RNA synthesis by interacting with the internal ribosome entry site in the 5″ untranslated region. J Virol 94:e00282-20. https://doi.org/10.1128/JVI.00282-20.
13. Cao L, Liu S, Li Y, Yang G, Luo Y, Li S, Du H, Zhao Y, Wang D, Chen J, Zhang Z, Li M, Ouyang S, Gao X, Sun Y, Wang Z, Yang L, Lin R, Wang P, You F. 2019. The nuclear matrix protein SAFA surveils viral RNA and facilitates immunity by activating antiviral enhancers and super-enhancers. Cell Host Microbe 26:369–384.e8. https://doi.org/10.1016/j.chom.2019.08.010.
14. Liu N, Dai Q, Zheng G, He C, Parisien M, Pan T. 2015. N(6)-methyladenosine-dependent RNA structural switches regulate RNA-protein interactions. Nature 518:560–564. https://doi.org/10.1038/nature14234.
15. Zaccara S, Ries RJ, Jaffrey SR. 2019. Reading, writing and erasing mRNA methylation. Nat Rev Mol Cell Biol 20:608–624. https://doi.org/10.1038/s41580-019-0168-5.
16. Wang X, Lu Z, Gomez A, Hon GC, Yue Y, Han D, Fu Y, Parisien M, Dai Q, Jia G, Ren B, Pan T, He C. 2014. N6-methyladenosine-dependent regulation of messenger RNA stability. Nature 505:117–120. https://doi.org/10.1038/nature12730.
17. Hazra D, Chapat C, Graille M. 2019. m(6)A mRNA destiny: chained to the rhYTHm by the YTH-containing proteins. Genes (Basel) 10:49. https://doi.org/10.3390/genes10010049.
18. Roundtree IA, Luo GZ, Zhang Z, Wang X, Zhou T, Cui Y, Sha J, Huang X, Guerrero L, Xie P, He E, Shen B, He C. 2017. YTHDC1 mediates nuclear export of N(6)-methyladenosine methylated mRNAs. Elife 6:e31311. https://doi.org/10.7554/eLife.31311.
19. Zheng Q, Hou J, Zhou Y, Li Z, Cao X. 2017. The RNA helicase DDX46 inhibits innate immunity by entrapping m(6)A-demethylated antiviral transcripts in the nucleus. Nat Immunol 18:1094–1103. https://doi.org/10.1038/ni.3830.
20. Xu X, Wang L, Liu Y, Shi X, Yan Y, Zhang S, Zhang Q. 2022. TRIM56 overexpression restricts porcine epidemic diarrhoea virus replication in Marc-145 cells by enhancing TLR3-TRAF3-mediated IFN-beta antiviral response. J Gen Virol 103. https://doi.org/10.1099/jgv.0.001748.
21. Murakami S, Jaffrey SR. 2022. Hidden codes in mRNA: control of gene expression by m(6)A. Mol Cell 82:2236–2251. https://doi.org/10.1016/j.molcel.2022.05.029.
22. Bleichert F, Baserga SJ. 2007. The long unwinding road of RNA helicases. Mol Cell 27:339–352. https://doi.org/10.1016/j.molcel.2007.07.014.
23. Kadare G, Haenni AL. 1997. Virus-encoded RNA helicases. J Virol 71:2583–2590. https://doi.org/10.1128/JVI.71.4.2583-2590.1997.
24. Xia H, Wang P, Wang GC, Yang J, Sun X, Wu W, Qiu Y, Shu T, Zhao X, Yin L, Qin CF, Hu Y, Zhou X. 2015. Human enterovirus nonstructural protein 2CATPase functions as both an RNA helicase and ATP-independent RNA chaperone. PLoS Pathog 11:e1005067. https://doi.org/10.1371/journal.ppat.1005067.
25. Yang J, Cheng Z, Zhang S, Xiong W, Xia H, Qiu Y, Wang Z, Wu F, Qin CF, Yin L, Hu Y, Zhou X. 2014. A cypovirus VP5 displays the RNA chaperone-like

activity that destabilizes RNA helices and accelerates strand annealing. Nucleic Acids Res 42:2538–2554. https://doi.org/10.1093/nar/gkt1256.
26. Valente ST, Goff SP. 2006. Inhibition of HIV-1 gene expression by a fragment of hnRNP U. Mol Cell 23:597–605. https://doi.org/10.1016/j.molcel.2006.07.021.
27. Hu X, Wu X, Ding Z, Chen Z, Wu H. 2023. Characterization and functional analysis of chicken dsRNA binding protein hnRNPU. Dev Comp Immunol 138:104521. https://doi.org/10.1016/j.dci.2022.104521.
28. Piñol-Roma S, Dreyfuss G. 1993. hnRNP proteins: localization and transport between the nucleus and the cytoplasm. Trends Cell Biol 3:151–155. https://doi.org/10.1016/0962-8924(93)90135-n.
29. Piñol-Roma S, Dreyfuss G. 1992. Shuttling of pre-mRNA binding proteins between nucleus and cytoplasm. Nature 355:730–732. https://doi.org/10.1038/355730a0.
30. Perry AK, Chen G, Zheng D, Tang H, Cheng G. 2005. The host type I interferon response to viral and bacterial infections. Cell Res 15:407–422. https://doi.org/10.1038/sj.cr.7290309.
31. Cao L, Ge X, Gao Y, Ren Y, Ren X, Li G. 2015. Porcine epidemic diarrhea virus infection induces NF-kappaB activation through the TLR2, TLR3 and TLR9 pathways in porcine intestinal epithelial cells. J Gen Virol 96:1757–1767. https://doi.org/10.1099/vir.0.000133.
32. Cao L, Ge X, Gao Y, Herrler G, Ren Y, Ren X, Li G. 2015. Porcine epidemic diarrhea virus inhibits dsRNA-induced interferon-beta production in porcine intestinal epithelial cells by blockade of the RIG-I-mediated pathway. Virol J 12:127. https://doi.org/10.1186/s12985-015-0345-x.
33. Ding Z, Fang L, Jing H, Zeng S, Wang D, Liu L, Zhang H, Luo R, Chen H, Xiao S. 2014. Porcine epidemic diarrhea virus nucleocapsid protein antagonizes beta interferon production by sequestering the interaction between IRF3 and TBK1. J Virol 88:8936–8945. https://doi.org/10.1128/JVI.00700-14.
34. Zhang J, Yuan S, Peng Q, Ding Z, Hao W, Peng G, Xiao S, Fang L. 2022. Porcine epidemic diarrhea virus nsp7 inhibits interferon-induced JAK-STAT signaling through sequestering the interaction between KPNA1 and STAT1. J Virol 96:e0040022. https://doi.org/10.1128/jvi.00400-22.
35. Jin H, Zhou L, Ge X, Zhang H, Zhang R, Wang C, Wang L, Zhang Z, Yang H, Guo X. 2017. Cellular DEAD-box RNA helicase 18 (DDX18) Promotes the PRRSV Replication via Interaction with Virus nsp2 and nsp10. Virus Res 238:204–212. https://doi.org/10.1016/j.virusres.2017.05.028.
36. Setoh YX, Periasamy P, Peng NYG, Amarilla AA, Slonchak A, Khromykh AA. 2017. Helicase domain of West Nile virus NS3 protein plays a role in inhibition of type I interferon signalling. Viruses-Basel 9:326. https://doi.org/10.3390/v9110326.
37. Xu LH, Huang M, Fang SG, Liu DX. 2011. Coronavirus infection induces DNA replication stress partly through interaction of its nonstructural protein 13 with the p125 subunit of DNA polymerase delta. J Biol Chem 286:39546–39559. https://doi.org/10.1074/jbc.M111.242206.
38. Cui L, Ma R, Cai J, Guo C, Chen Z, Yao L, Wang Y, Fan R, Wang X, Shi Y. 2022. RNA modifications: importance in immune cell biology and related diseases. Signal Transduct Target Ther 7:334. https://doi.org/10.1038/s41392-022-01175-9.
39. Lee Y, Choe J, Park OH, Kim YK. 2020. Molecular mechanisms driving mRNA degradation by m(6)A modification. Trends Genet 36:177–188. https://doi.org/10.1016/j.tig.2019.12.007.
40. Chen X, Zhou X, Wang X. 2022. m(6)A binding protein YTHDF2 in cancer. Exp Hematol Oncol 11:21. https://doi.org/10.1186/s40164-022-00269-y.
41. Gokhale NS, McIntyre ABR, McFadden MJ, Roder AE, Kennedy EM, Gandara JA, Hopcraft SE, Quicke KM, Vazquez C, Willer J, Ilkayeva OR, Law BA, Holley CL, Garcia-Blanco MA, Evans MJ, Suthar MS, Bradrick SS, Mason CE, Horner SM. 2016. N6-methyladenosine in Flaviviridae viral RNA genomes regulates infection. Cell Host Microbe 20:654–665. https://doi.org/10.1016/j.chom.2016.09.015.
42. Xu J, Cai Y, Ma Z, Jiang B, Liu W, Cheng J, Guo N, Wang Z, Sealy JE, Song C, Wang X, Li Y. 2021. The RNA helicase DDX5 promotes viral infection via regulating N6-methyladenosine levels on the DHX58 and NFkappaB transcripts to dampen antiviral innate immunity. PLoS Pathog 17:e1009530. https://doi.org/10.1371/journal.ppat.1009530.
43. Jin J, Xu C, Wu S, Wu Z, Wu S, Sun M, Bao W. 2022. m(6)A demethylase ALKBH5 restrains PEDV infection by regulating GAS6 expression in porcine alveolar macrophages. Int J Mol Sci 23:6191. https://doi.org/10.3390/ijms23116191.
44. Sun P, Wu H, Huang J, Xu Y, Yang F, Zhang Q, Xu X. 2018. Porcine epidemic diarrhea virus through p53-dependent pathway causes cell cycle arrest in the G0/G1 phase. Virus Res 253:1–11. https://doi.org/10.1016/j.virusres.2018.05.019.
45. Xu X, Xu Y, Zhang Q, Yang F, Yin Z, Wang L, Li Q. 2019. Porcine epidemic diarrhea virus infections induce apoptosis in Vero cells via a reactive oxygen species (ROS)/p53, but not p38 MAPK and SAPK/JNK signalling pathways. Vet Microbiol 232:1–12. https://doi.org/10.1016/j.vetmic.2019.03.028.